An Artificial Neural Network Model for Dynamic Analysis of RC Buildings Subjected to Near-Fault Ground Motions Having Forward Directivity

Alireza Mortezaei[1] and Hamid Reza Ronagh[2]*

1. Assistant Professor, Department of Civil Engineering, Semnan Branch, Islamic Azad University, Semnan, Iran, * Corresponding Author; e-mail: a.mortezaei@semnaniau.ac.ir
2. Senior Lecturer, School of Civil Engineering, University of Queensland, Brisbane, Australia

Received: 08/08/2011
Accepted: 07/05/2012

ABSTRACT

The near field region of an earthquake is considered to be the region within several kilometers of the extension to the ground surface of the rupture plane. Recordings from recent earthquakes have provided facts that ground motions in the near field of a rupturing fault can contain a large energy, or "directivity," pulse. The objective of this study is to investigate the sufficiency of Artificial Neural Networks (ANN) to determine the three dimensional dynamic response of buildings under the near-fault earthquakes. For this purpose, four ANN models are proposed to estimate the fundamental periods, base shear force, base bending moments and roof displacement of buildings in two directions. The same input layer was submitted to different types of ANN models and the results monitored. A training set of 168 and a validation set of 21 buildings were produced from dynamic response of RC buildings under the near-fault earthquakes by IDARC program. It was demonstrated that the neural network-based approach is highly successful to determine the response of RC buildings subjected to near-fault earthquakes.

Keywords:
Dynamic analysis;
RC buildings;
Artificial neural networks;
Near-fault earthquake

1. Introduction

Considerable discussion has taken place on the effect of ground motions on structural systems. As distinguished from ground motions recorded at moderate distances from the contributing fault, near-fault motions contain intense, relatively long duration pulses corresponding to the fault rupture process. Impulsive type motions can cause significant damage during an earthquake, especially to structures with natural periods close to those of the pulse [1].

After the 1971 San Fernando earthquake, engineers and seismologists realized the potential damage that may occur due to the effects of near-fault ground motions on structures. The damage observed during the 1994 Northridge, California, the 1995 Kobe, Japan, the 1999 Izmit, Turkey, the 2003 Bam, Iran, and the 2011 Japan earthquakes proved the engineers' theory that structures located within the near-fault area sustain more severe damages than structures located outside of this zone. These earthquakes provided a wealth of new information about the behavior of engineered structures because the respective epicenters were in urban settings.

Bertero et al [2] were among the pioneers who studied velocity pulses and their effects on structures. After the 1994 Northridge and 1995 Kobe earthquakes, many engineers and seismologists began to study the components of velocity pulses. If the conditions of forward directivity are satisfied, the record will be shorter in duration, higher in frequency content, and the majority of the seismic energy will be delivered in a large velocity pulse.

The objective of this research is to use the wealth of recent ground motion data to improve the understanding of the response of typical reinforced concrete buildings to pulse-type ground motions that

result from forward-directivity effects and also, discuss the adequacy of *ANN* as a secure and faster method to be used in predicting the dynamic responses of *RC* buildings.

2. Characteristics of Near-Fault Ground Motions

The near-fault region of an earthquake can be defined as any area in the close neighborhood of the fault rupture surface. In the near-fault, the ground shaking is influenced by a number of factors. Besides strong shaking, the characteristics of near-fault ground motions are linked to the fault geometry and the orientation of the traveling seismic waves [3]. Vertical strike-slip faults can produce a directivity effect, and dip-slip faults can produce directivity effects as well as hanging wall effects. Hanging wall effects are felt on the hanging wall of a fault (the earth above a vertically dipping fault), and are due to the proximity of much of the fault to hanging wall sites. Directivity effects can be classified as forward, reverse, and neutral. Forward directivity is when the direction of the rupture propagates toward the site, while reverse directivity is when the rupture progresses away from the site. Neutral directivity is when the site is perpendicular to the ruptured fault [4]. Within the research community, the term "directivity effects" has come to mean "forward directivity effects" because forward directivity is more likely to be responsible for the ground motions that cause damage. Figure (1) portrays the three zones of directivity, with the star representing the epicenter and the black line indicating the fault.

When a fault rupture propagates toward a site at a velocity close to that of the shear wave velocity, an accumulation of most of the energy of the seismic radiation of the fault can arrive at the site as a single long-period pulse. This is called a directivity pulse [3]. The rupture is broken into sub-faults; beginning at the epicenter, the rupture propagates along the fault in the direction of the arrow toward Site *A*. Because the velocity of the shear waves is close to the rupture velocity, the energy of the forward direction arrives within a short time period. Forward directivity effects only occur when the rupture propagates toward the site, and the direction of slip on the fault is aligned with the site. Not all near-fault locations will experience forward rupture directivity effects in a given event. It can be seen by the model that Site *B*, see Figure (2), will experience a lengthening of the time between the appearances of the waves; thus, the record at Site *B* will have a long duration but not a velocity pulse.

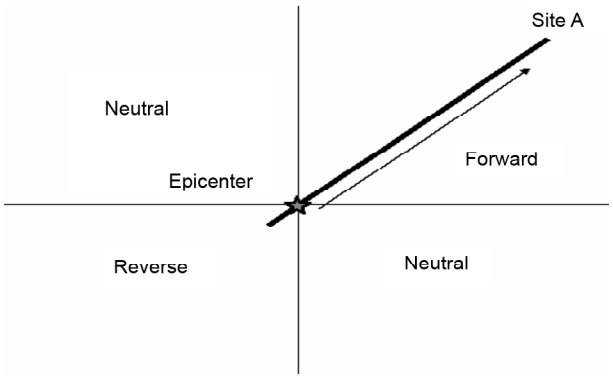

Figure 1. Zones of directivity [4].

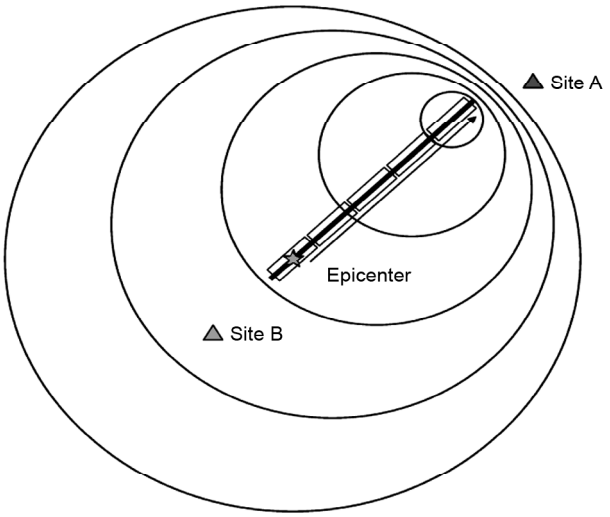

Figure 2. Directivity pulse accumulates as rupture propagates to right [4].

Forward directivity effects can be felt for both strike-slip faults and dip-slip faults. On a strike-slip fault, the directivity effects are mostly concentrated away from the hypocenter because the energy builds up as the shear waves travel away from the point of dislocation toward the site. A dip-slip fault produces forward directivity effects at the sites located around the surface exposure of the fault [4]. Although the geometry of a fault is usually well known, the direction of rupture is unpredictable. Therefore, it is recommended that all buildings that fall within the near-fault of an active fault be designed for a possible velocity pulse.

The velocity and displacement time histories of

typical near-fault ground motions having forward-directivity effects (Rinaldi record of 1994 Northridge earthquake) are compared to that of ordinary far-fault motion (Taft record of 1952 Kern County earthquake) in Figure (3). High-velocity pulses are quite distinctive for Rinaldi; such pulses do not exist in a typical far-fault ground motion like Taft.

3. Research Significance

Research over the past decade has shown that pulse-type earthquake ground motions that result from forward-directivity effects can result in significant damage to structures. The objective of first part of this research is to use the wealth of recent ground motion data to improve the understanding of the response of typical reinforced concrete buildings to pulse-type ground motions that result from forward-directivity effects.

Although three dimensional nonlinear dynamic analyses of *RC* buildings provide valuable information about their behavior, they are expensive and time-consuming. Using *ANN* based models; it is possible, at comparatively low cost and effort, to predict the response of *RC* structures provided that adequate input layers with correct input parameters are chosen and trained. They also enable the designer to rapidly evaluate the three-dimensional response of buildings during the preliminary design stage. In these models, the goal is to drastically reduce the computational effort. In this study, *ANN*

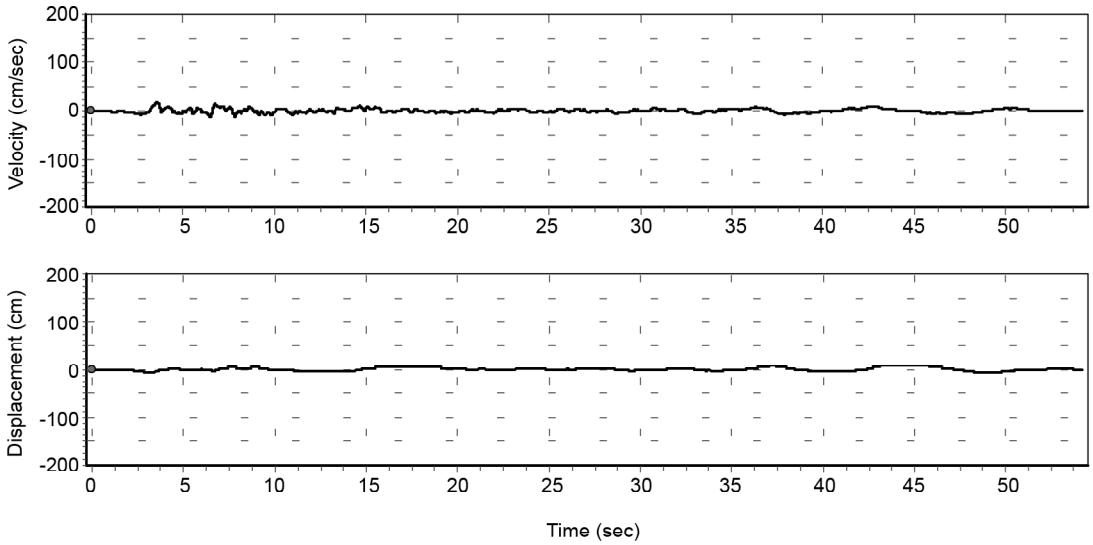

(a) Taft Record of the 1952 Kern County Earthquake

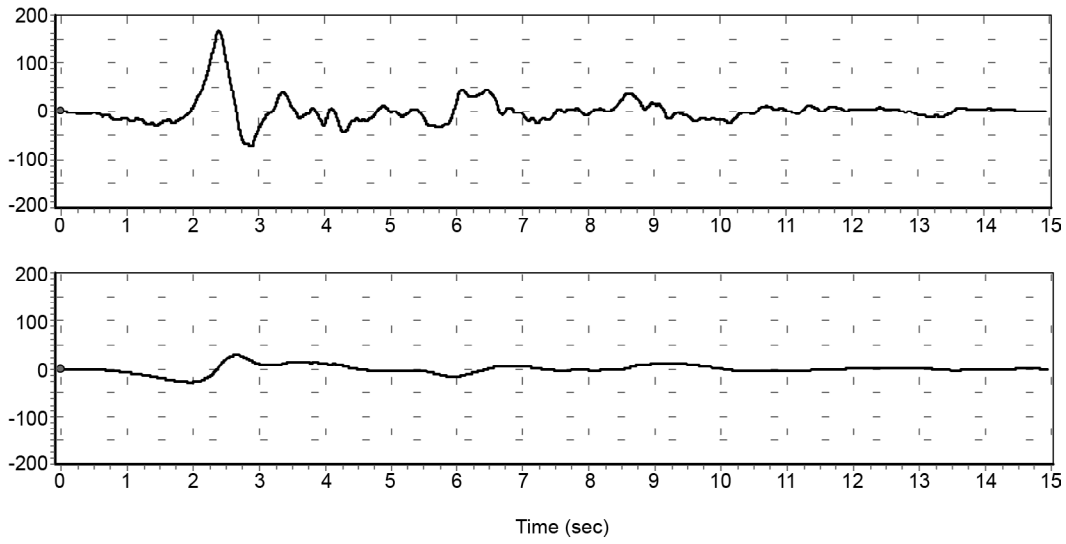

(b) Rinaldi Record of the 1994 Northridge Earthquake

Figure 3. Typical velocity and displacement time histories of (a) far-fault, (b) near-fault (forward-directivity) ground motions.

based models were employed as alternatives to determine the three dimensional dynamic response of buildings, in terms of fundamental periods in two directions, maximum values of base shear forces, dissipated energy and drift angles in two directions.

4. Description of Buildings Used for Evaluation

Eight existing reinforced concrete dual system (moment-resisting frame with shear walls) buildings of 3, 5, 6, 9, 10, 14, 16 and 19 stories were selected as representative case studies to evaluate their seismic demands when subjected to near-fault ground motions with forward directivity, and to compare their respective responses to typical far-fault ground motions. These buildings were designed in compliance to the Iranian Code of Practice for Seismic Resistant Design of Buildings [5]. The rectangular plan of all buildings measures 30*m* by 25*m*. The floor plans and elevation views of the buildings with beam and column sections are shown in Figure (4). The columns are embedded into the mat foundation, essentially restraining displacements and rotations in all directions. The buildings are assumed with a damping ratio of 5% in all modes, and the floors as rigid diaphragms with infinite in-plane stiffness. The sections of structural elements are square and rectangular, and their dimensions are logically changed at different stories. The slab thickness is 10*cm*. For the sake of clarity, the column and beam dimensions and reinforcement of the 10-story building have been mentioned in Tables (1) and (2). Story heights of buildings are assumed to be constant except for the 1st story. The modulus of elasticity (Young's modulus) E=30kN/mm^2, Poisson's ratio v=0.20 and the mass density ρ=24kN/m^3 are assumed in all models. The uniaxial strength for nonlinear modeling of the concrete is considered to be 35*MPa*. The rebar is modeled as steel with yield strength of 400*MPa* and an ultimate strength of 600*MPa*.

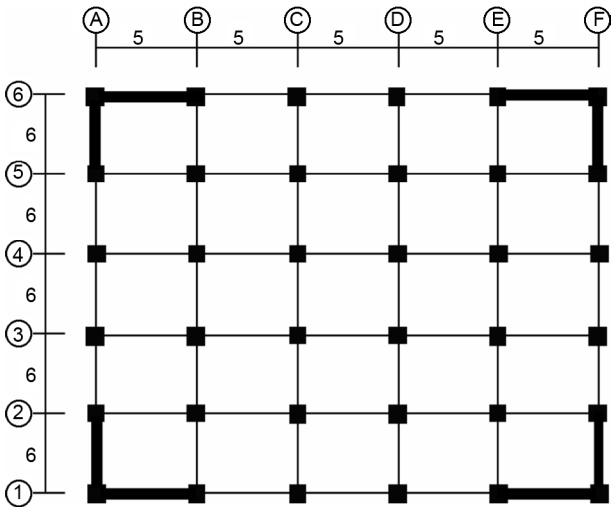

Figure 4. Structural configuration of evaluated buildings (units: meter).

Permanent and imposed loads are assumed to be: dead load of story level, 5.5*kPa*; dead load of roof, 6*kPa*; dead load of partitions, 1*kPa*; dead load of external walls, 2.5*kPa*; live load of story levels, 2*kPa*; and live load of roof, 1.5*kPa*.

5. Ground Motion Database

The ground motion database compiled for nonlinear time-history analyses constitutes a representative number of far-fault and near-fault ground motions from a variety of tectonic environments. A total of 14 records were selected to cover a range

Table 1. Dimensions and amounts of reinforcement of columns in 10-story building.

Building	Storey	Corner Column		Perimeter Column		Internal Column	
		Dimensions (cm)	Reinforcement (mm^2)	Dimensions (cm)	Reinforcement (mm^2)	Dimensions (cm)	Reinforcement (mm^2)
10 Storey	1	60×60	2100	60×60	1880	60×60	1930
	2	60×60	1200	60×60	1200	60×60	1200
	3	60×60	1200	60×60	1200	60×60	1200
	4	60×60	1200	60×60	1200	60×60	1200
	5	50×50	910	50×50	1335	50×50	950
	6	50×50	840	50×50	910	50×50	840
	7	50×50	840	50×50	900	50×50	840
	8	40×40	775	40×40	1070	40×40	840
	9	40×40	600	40×40	880	40×40	600
	10	40×40	600	40×40	880	40×40	600

Table 2. Dimensions and amounts of reinforcement of beams in 10 story-building model.

Storey	Beams of external frames						Beams of internal frames					
	Type 4			Type 3			Type 2			Type 1		
	Dimensions (cm) w.×h.	Reinforcement (mm^2)		Dimensions (cm) w.×h.	Reinforcement (mm^2)		Dimensions (cm) w.×h.	Reinforcement (mm^2)		Dimensions (cm) w.×h.	Reinforcement (mm^2)	
		Bottom	Top		Bottom	Top		Bottom	Top		Bottom	Top
1	60×50	1316	1664	60×50	1108	1583	60×50	1176	1670	60×50	1104	1593
2	60×50	1685	2071	60×50	1488	1972	60×50	1532	2093	60×50	1484	1981
3	60×50	1728	2141	60×50	1566	2054	60×50	1568	2176	60×50	1562	2059
4	60×50	1764	2181	60×50	1564	2043	60×50	1600	2223	60×50	1557	2055
5	50×45	1484	1931	50×45	1276	1823	50×45	1298	1965	50×45	1270	1835
6	50×45	1393	1860	50×45	1221	1770	50×45	1203	1903	50×45	1214	1778
7	50×45	1287	1737	50×45	1076	1607	50×45	1103	1779	50×45	1066	1625
8	40×40	947	1424	40×40	711	1334	40×40	738	1449	40×40	702	1352
9	40×40	665	1157	40×40	529	1100	40×40	570	1190	40×40	533	1110
10	40×40	495	760	40×40	473	727	40×40	502	773	40×40	492	757

of frequency content, duration and amplitude. Near-fault records were chosen so as to consider the presence of forward-directivity effects. Hence the assembled database can be investigated in two sub-data sets. The first set contains seven ordinary far-fault ground motions recorded within 90*km* of the causative fault plane from earthquakes in the magnitude (*MW*) range of 6.5 to 7.4. The second set includes seven near-fault ground motions characterized with forward-directivity effect. These records are from earthquakes having a magnitude (*MW*) range of 6.5 to 7.4, and recorded at closest fault distance of 0.0 to 10*km*. Information relevant to the ground motion data sets, including station, component of earthquake and peak ground acceleration (*PGA*), peak ground velocity (*PGV*), and peak ground displacement (*PGD*) of records are presented in Tables (3) and (4).

Utilized in this study is a data processing technique proposed by Iwan et al [6] and refined in Reference [7] to recover the long-period components from near-fault accelerograms. This process

Table 3. Far-fault ground motion database.

No.	Earthquake	Year	Station	Comparison	M_w	Displacement (km)	PGA (g)	PGV (cm/s)	PGD (cm)
1	Kern County	1952	Taft	111	7.4	81	0.17	17.47	8.83
2	Tabas	1978	Dayhook	TR	7.4	107	0.4	26.17	9.1
3	Imperial Valley	1979	Calexico	225	6.5	90.6	0.27	21.23	8.98
4	Loma Prieta	1989	Presidio	000	6.9	83.1	0.099	12.91	4.32
5	Loma Prieta	1989	Cliff House	90	6.9	84.4	0.107	19.78	5.06
6	Manjil	1990	Abbar	L	7.3	74	0.51	42.46	14.92
7	Kocaeli	1999	Ambarli	90	7.4	78.9	0.18	33.22	25.84

Table 4. Near-fault ground motion database.

No.	Earthquake	Year	Station	Comparison	M_w	Displacement (km)	PGA (g)	PGV (cm/s)	PGD (cm)
1	Tabas	1978	Tabas	TR	7.4	3	0.85	121.22	95.06
2	Loma Prieta	1989	LGPC	00	7.0	1.3	0.56	94.71	41.13
3	Cape Mendocino	1992	Petrolia	90	7.1	9.5	0.66	89.68	28.99
4	Erzincan	1992	Erzincan	NS	6.9	2	0.51	83.95	27.66
5	Northridge	1994	Rinaldi	228	6.7	7.1	0.83	166.03	28.15
6	Northridge	1994	Sylmar	360	6.7	6.4	0.84	129.3	31.92
7	Bam	2003	Bam	L1	6.5	7	1.09	131.26	89.24

has been extensively elaborated in Reference [8] and [9].

6. Seismic Response Evaluation of Buildings

Totally, 280 nonlinear time history (*NTH*) analyses were conducted on the eight buildings Inter-story drift ratio (*IDR*), defined as the relative displacement between two consecutive story levels, displacements at different story levels, base shear force, dissipated energy and shear forces at different story levels are used as the primary measure of seismic demand. Additional demand measures, such as component and story ductility were also investigated. In general, there is a reasonable correlation between the inter-story drift demands and component/story-level ductility demands; hence the results are not included here. The peak inter-story drift profiles obtained from *NTH* analyses of the some buildings subjected to the two sets of ground motions (i.e., far-fault motions, near-fault motions with forward directivity) are presented in Figure (5).

For the 3-story building, far-fault motions produce

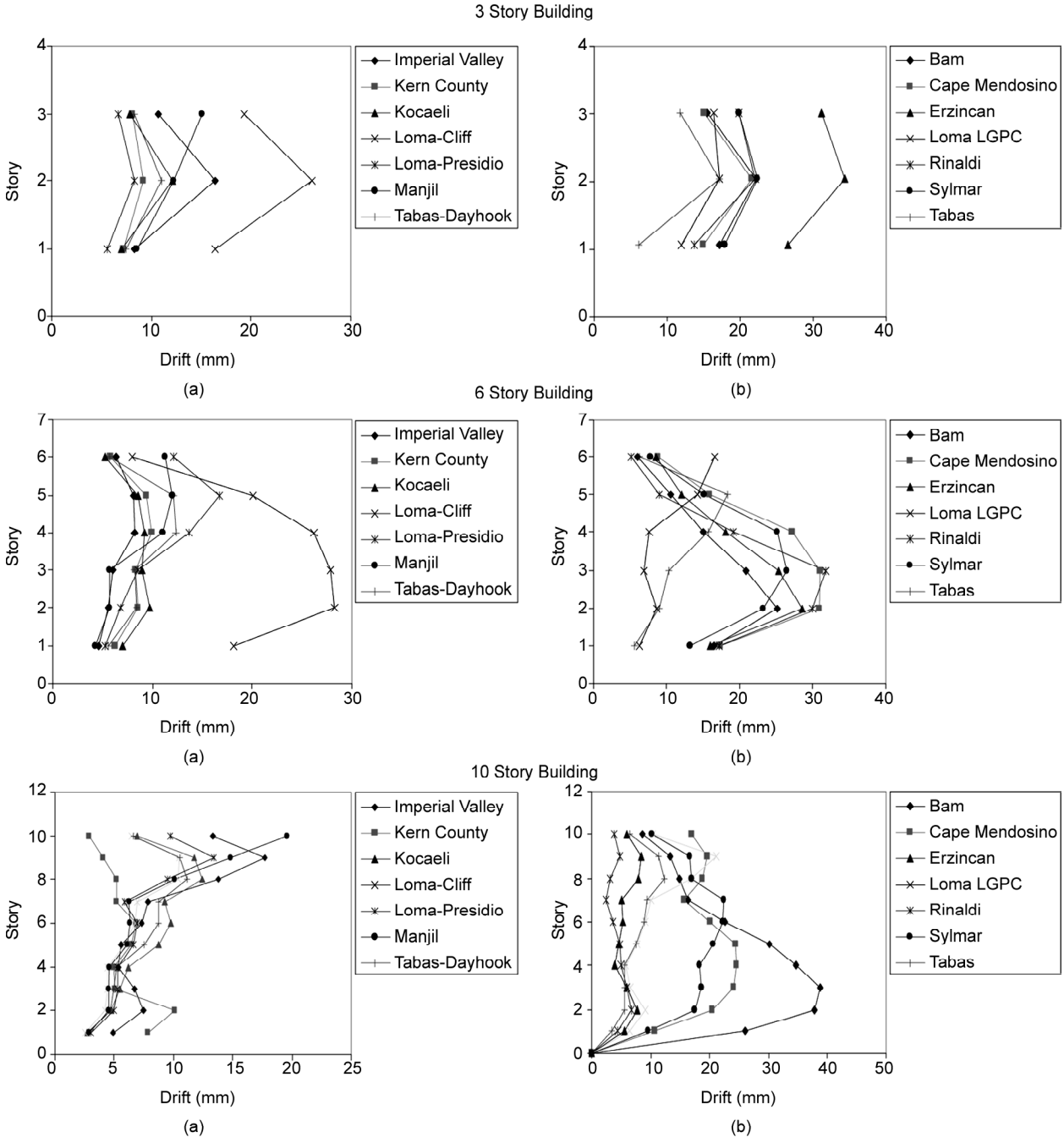

Figure 5. Maximum inter-story drift for each building subjected to (a) far-fault earthquakes, (b) near-fault earthquakes with forward directivity.

a nearly uniform inter-story drift demand for most records, with the exception of the Loma-Cliff record, which triggers higher-mode effects resulting in increased demands in the upper stories. In case of near-fault records, they impose higher demands in comparison to far-fault records though the maximum drift is generally concentrated at the middle story levels. The largest demand is caused by the Erzincan record, which produced 34.4*mm* inter-story drift at the second story.

For the 6-story building, the maximum story demand for far-fault records is observed to be either at the second or third story levels and depends on the frequency content of the motion. Though similar observations hold for near-fault records, the demands at the intermediate levels are much higher. Of the entire data set, the Rinaldi record generated the highest demand (31.8*mm* interstory drift) at the third story.

For the 10-story building, the Bam record generated the highest demand (38.71*mm* inter-story drift) at the third story level. Higher-mode effects are predominant in many of the near-fault records causing a shift in demands from the lower to upper stories.

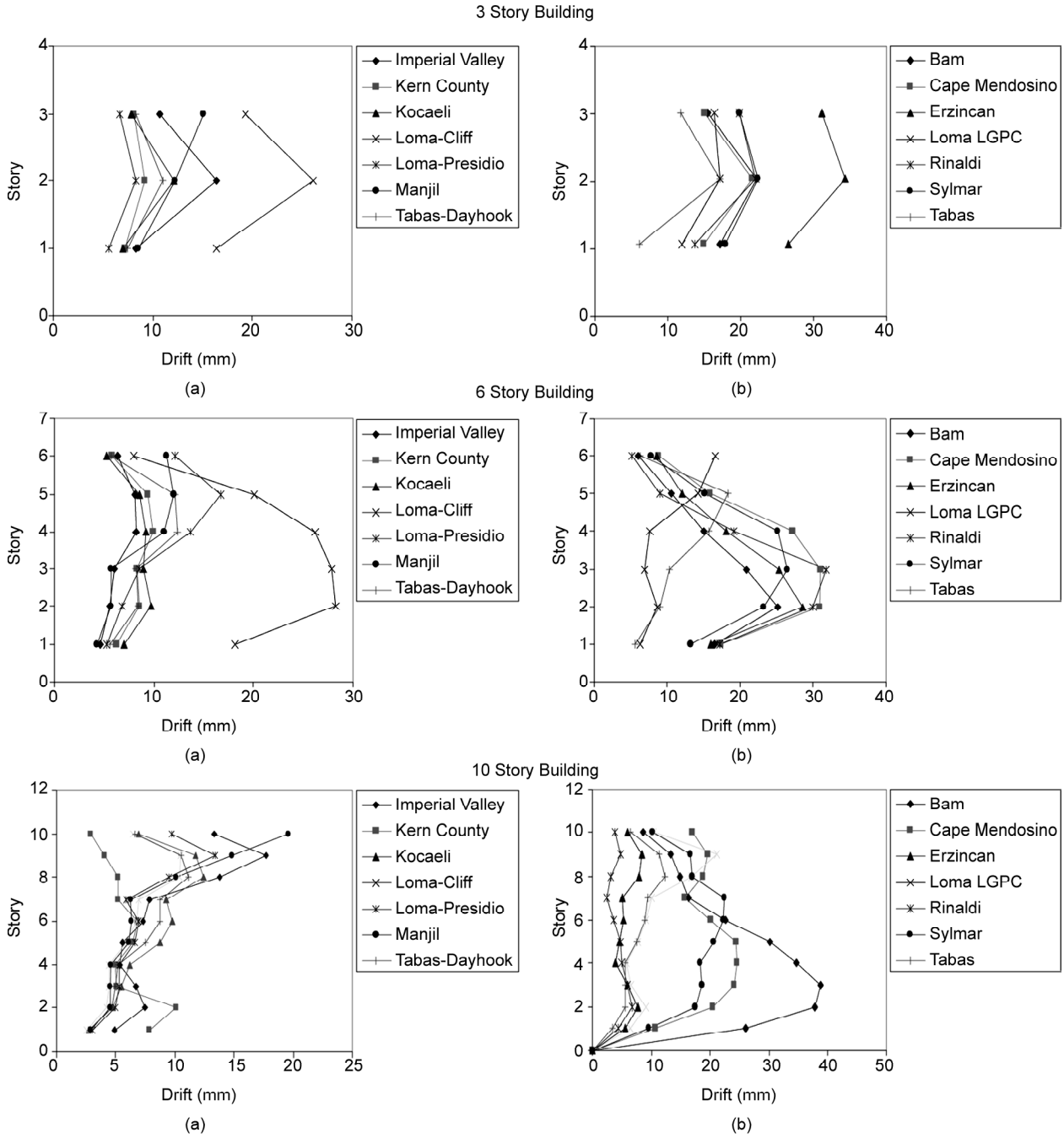

Figure 5. (Continue)

For the 14-story building, the maximum story demand for far-fault records is observed to be either at the 7^{th} or 8^{th} story levels and depends on the frequency content of the motion. Though similar observations hold for near-fault records, the demands at the upper levels are much higher. Of the entire data set, the Bam record generated the highest demand (20.56*mm* inter-story drift) at the 9^{th} story. Similar results were observed for 16- and 19-story buildings. In both buildings, Bam record generated the highest demand (21.1*mm* and 25.32*mm* inter-story drift for 16- and 19-story buildings, respectively).

The variation in story demand for the far-fault records is less significant. While higher-mode effects are expected to contribute to the response of the 6- and 10-story buildings, the response of the 3-story building demonstrates that even for low-rise buildings, higher-mode effects could be significant.

7. Artificial Neural Networks

Artificial neural networks are computing systems that simulate the organic neural systems of human brain. *ANNs* are structures deliberately designed to imitate and use the organizational principles observed in the brain [10]. They are based on a simplified modeling of the brain's biological functions exhibiting the ability to learn, think, remember, reason, and solve problems. Artificial neural networks can be most adequately characterized as computational models with particular properties such as the ability to adapt or to learn, to generalize or to cluster or organize data, in which an operation is based on parallel processing. It can be applied to many fields. *ANN* has been applied to a wide range of civil engineering problems [11].

In this study, the *ANN* based models were applied to predict the three-dimensional response of buildings in terms of fundamental periods, maximum values of roof displacements and base shear forces and dissipated energy in the time domain. Hence, the general description of *ANN* in the following sections will be concentrated on its capacity to establish a functional relationship between input and output data. Firstly, the general structure of *ANN* will be introduced. The methods used for training, cross validating and testing *ANN* models are then presented. Thirdly, a mathematical expression of *ANN* models will be described, and its inherent advantages over the conventional regression analysis will be discussed.

8. Structure of Neural Network

A typical structure of an *ANN* model can be established by Figure (6), in which the left column is the input layer, the right column is the output layer, and in between the input and output layers, is a hidden layer. Normally, there could be more than one hidden layer.

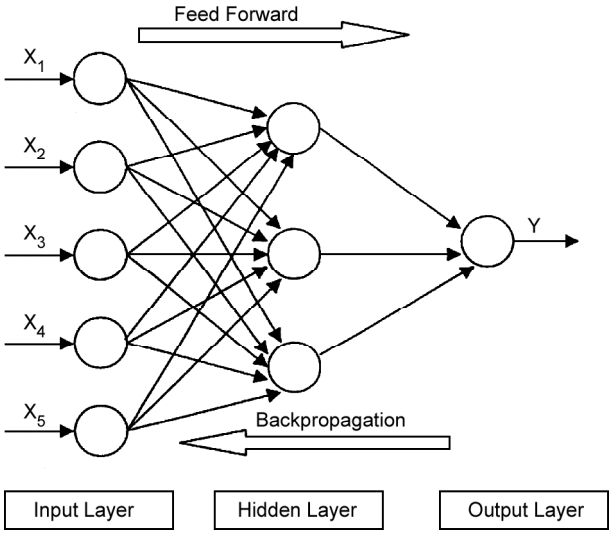

Figure 6. General structure of an artificial neural network.

In each layer, there are numerous Processing Elements (PE). The number of PEs in the input layer is equal to the number of input parameters, while the number in the output layer is equal to the number of output parameters. The significant task in an *ANN* model is to verify the number of PEs in the hidden layer, which affects the correctness of the model. Each processing element has several inputs and one output. The relation between input, x_j, and output, y_p, of a single *PE* can be expressed as [12]:

$$y_p = f\left(\sum_{j=1}^{T} \omega_p^j x_j + a_p\right) \qquad (j = 1, 2, ..., T) \tag{1}$$

where ω_p^j is weights, a_p is a constant (usually referred to as threshold), $f(\cdot)$ is called the activation function, which could be a sigmoid function or hyperbolic tangent function, etc. The *PEs* in the hidden layer will obtain data from only the input layer. Similarly, the *PEs* in the output layer will only obtain data from the hidden layer.

Once the topology of an *ANN* model is decided, the next task is to determine the values of all the weights, which will be resulted in the following

section. This process consists of three steps, namely training, cross validation and test. The details of this can be seen in the reference [12].

9. Background

Backpropagation is a common method of teaching artificial neural networks how to perform a given task. The weights of each unit must be adjusted in such a way that the error between the desired output and the actual output is reduced. This process requires that the neural network compute the error derivative of the weights (*EW*). In other words, it must calculate how the error changes as each weight is increased or decreased slightly.

The back propagation algorithm is the most widely used method for determining the *EW*. The algorithm computes each *EW* by first computing the *EA*, the rate at which the error changes as the activity level of a unit is changed. For output units, the *EA* is the difference between the actual and the desired output. To compute the *EA* for a hidden unit in the layer just before the output layer, firstly, all the weights between that hidden unit and the output units to which it is connected are identified. Then, those weights are multiplied by the *EAs* of those output units and added the products. This sum equals the *EA* for the chosen hidden unit. After calculating all the *EAs* in the hidden layer just before the output layer, the *EAs* for other layers are computed in like fashion, moving from layer to layer in a direction opposite to the way activities propagate through the network. This is what gives back propagation its name. Once the *EA* has been computed for a unit, it is straight forward to compute the *EW* for each incoming connection of the unit. The *EW* is the product of the *EA* and the activity through the incoming connection.

Assume that the transpose of the vector of input variables is $X_T = (x_1, x_2, \ldots, x_n)$, and the transpose of the vector of output variables is $Y_T = (y_1, y_2, \ldots, y_L)$. For an *ANN* model with one hidden layer with *m* number of *PEs* in the hidden layer, the mathematical expression of the j^{th} output variable is [12]:

$$y_j = f\left(\sum_{j=1}^{T} wd_j^i \psi_j(X) + c_j\right) \qquad (j = 1, \ldots, L) \qquad (2)$$

where w_j^i is the weight of the i^{th} *PE* in the hidden layer to the j^{th} *PE* in the output layer, c_j is a constant, $\psi_j(X)$ is the output of the i^{th} *PE* in the hidden layer, which is expressed as:

$$\psi_i(X) = f\left(\sum_{k=1}^{n} wc_i^k x_k \psi_j + b_i\right) \qquad (j = 1, \ldots, m) \qquad (3)$$

where w_i^k is the weight of the k^{th} input variable in the input layer to the i^{th} *PE* in the hidden layer, and b_i is a constant.

There are many ways to choose base functions, for example, trigonometric polynomials (Fourier series) and polynomials. Selecting suitable base functions is very important in function estimation. If the choice is not appropriate, there will be a non-vanishing error, no matter how big the number of base functions is. In the context of developing empirical formulae in structural design, the polynomial is a popular form, see Figure (7).

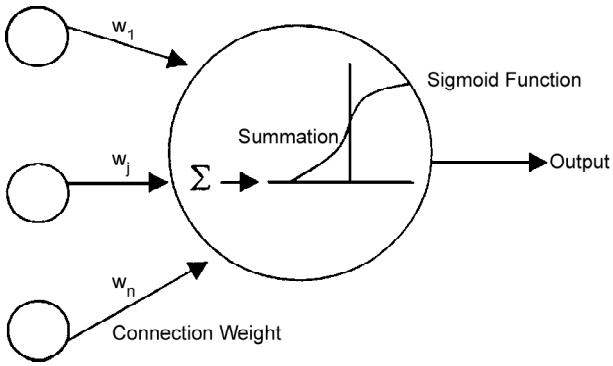

Figure 7. Processing neuron in ANN.

When a detailed description is lacking, a sigmoid function is often used. A sigmoid curve is produced by a mathematical function having an "*S*" shape and defined by the formula:

$$P(t) = \frac{1}{1 + e^{-t}} \qquad (4)$$

where *P* is a variable with respect to time *t* and *e* is Euler's number.

Conventionally, the learning process is used to determine appropriate interconnection weights, and the network is trained to make proper associations between the inputs and their corresponding outputs. Errors that arise during the learning process can be expressed in terms of mean square error (*MSE*) and are calculated using Eq. (5).

$$MSE = \left(\frac{1}{p}\right)\sum_j (t_j - o_j)^2 \qquad (5)$$

In addition, the sum of the squared error (*SSE*), the absolute fraction of variance (R^2) and mean absolute percentage error (*MAPE*) are calculated using Eqs. (6) to (8), respectively.

$$SSE = \sum_{j=1}^{p} (t_j - o_j)^2 \tag{6}$$

$$R^2 = 1 - \left(\frac{\sum_j (t_j - o_j)^2}{\sum_j (o_j)^2} \right) \tag{7}$$

$$MAPE = \frac{1}{p} \sum_{j}^{p} \left(\left| \frac{o_j - t_j}{o_j} \right| \times 100 \right) \tag{8}$$

where t_j is the target value of j^{th} pattern, o_j is the output value of j^{th} pattern, and p is the number of patterns.

10. ANN Models for Prediction of Nonlinear Dynamic Analysis

The *ANN* based models were used for predicting the three dimensional response of buildings. Building responses are in terms of fundamental periods in two directions, maximum values of base shear forces, dissipated energy and drift angles in two directions in the time domain. Four *ANN* models, which used the same input layer, were developed as shown in Figure (8).

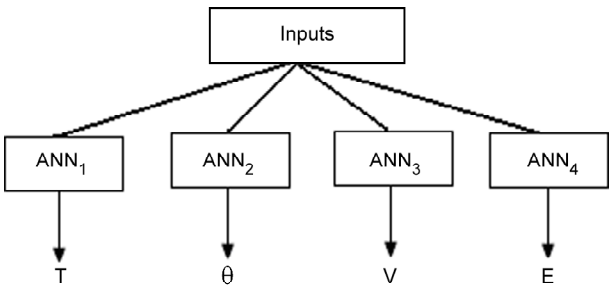

Figure 8. ANN models with the same inputs.

Main periods of building in two directions were simulated with the ANN_1 model, see Figure (9). The maximum of base shear forces, dissipated energy and drift angles time histories in two directions were simulated with the ANN_2, ANN_3 and ANN_4 models, respectively, see Figure (10). The ANN_2 model defines the drift angles in output layer. ANN_3 model defines the base shear force in output layer, and ANN_4 model defines the dissipated energy in output layer. The same input layer was used for three different outcomes in the ANN_2, ANN_3 and ANN_4 models.

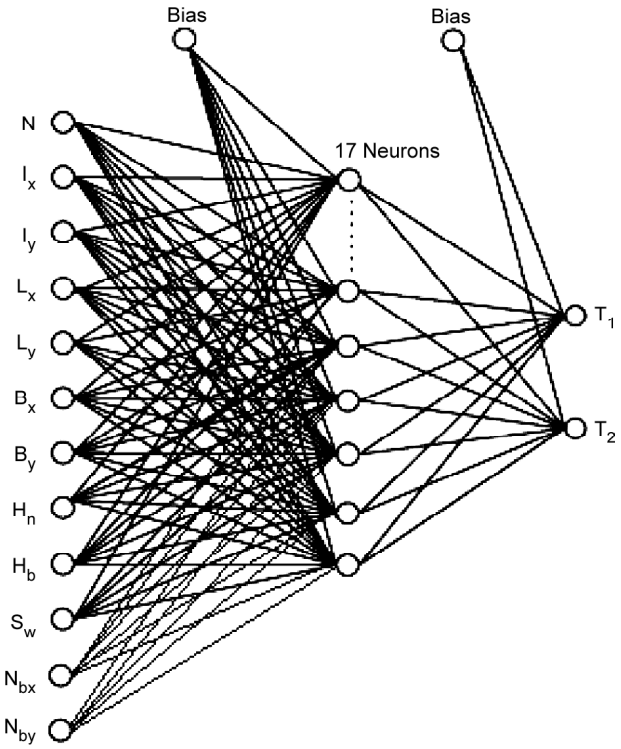

Figure 9. Architecture of proposed ANN_1 model.

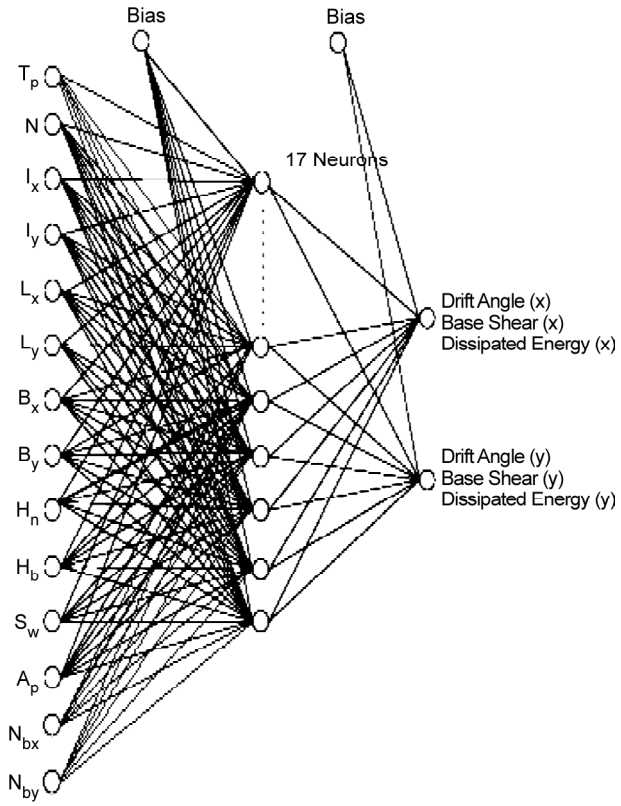

Figure 10. Architecture of proposed ANN_2, ANN_3, and ANN_4 models.

Nonlinear dynamic analyses of 280 reinforced concrete buildings subjected to seismic motions were carried out by the *IDARC* program [13]. The response of buildings is presented in terms of fundamental periods, maximum drift angles, base shear forces time histories and dissipated energy. For database, nonlinear dynamic analyses of these buildings were selected. These databases were divided into two sections: (1) the training set and (2) testing set. 175 of these data were utilized as the training set, 105 data were utilized as the testing set.

In time history dynamic analysis of buildings, a total of 14 records including seven far-fault earthquakes and seven near-fault earthquakes were selected to cover a range of frequency content, duration, and amplitude, see Tables (3) and (4). The peak acceleration of seismic records was normalized between 0.20 and 0.60*g* to simulate the *x*-direction and y-direction of buildings, respectively.

The inputs used for *ANN* models consisted of 14 data sets in terms of common properties of buildings and earthquakes, see Table (5). Although all inputs were utilized in the ANN_2, ANN_3 and ANN_4 models, only peak acceleration and pulse period were not used in the input layer of the ANN_1 model.

An important task in an *ANN* model is to determine the number of *PEs* in the hidden layer, which in turn affects the accuracy of the model. There is no general rule for selection of the number of neurons in a hidden layer and the number of the hidden layers. Hence, they are determined by trial and error in this study [14]. Numbers of different *NN* models with various hidden neurons are trained and tested for 3500 epochs. Each neural network model is started with different random weights. Suitable neural network models are selected according to the performance of training and testing sets. Therefore, the ANN_1 model is selected with 12 neurons in the input layer, 17 neurons in the hidden layer and two neurons in the output layer for determining the fundamental periods, see Figure (9). The ANN_2, ANN_3 and ANN_4 models are chosen with 14 neurons in input layer, 17 neurons in hidden layer and two neurons in output layer, for determining the drift angles, the base shear force, the dissipated energy, see Figure (10), using ANN_2, ANN_3 and ANN_4 models respectively. The quantity of inputs and outputs are normalized in the 0-1 range using normalization values given in Table (6).

Sensitivity analysis determines the influence of input variable contributions in neural networks sensitivity. Conventional sensitivity analysis involves varying each input variable across its entire range while holding all other input variables constant; in order that the individual contributions of each variable are assessed. The sensitivity analysis results show that among many parameters that potentially may affect the behavior, those shown in Table (5) are the most important ones affecting the network outputs.

A *MATLAB*-based computer program was utilized to train and test the neural network models based on

Table 5. Inputs for ANN models.

Notations	Inputs
A_p	Peak Acceleration
S_w	Shear Wall
I_x	Total Moment of Inertia (in x Direction)
I_y	Total Moment of Inertia (in y Direction)
H_n	Story Height
H_b	Story Height of Base Floor
L_x	Max Width of Bay in x Direction
L_y	Max Width of Bay in y Direction
B_x	Widths of Building in Plan in x Direction
B_y	Widths of Building in Plan in y Direction
N	Number of Stories
N_{bx}	Number of Bay in x Direction
N_{bx}	Number of Bay in y Direction
T_p	Pulse Period

Table 6. Range of parameters in the database and normalization values.

Parameter	Minimum	Maximum	Normalization Value
A_p (g)	0.2	0.6	1
S_w	0.0	1.0	1
I_x (m^4)	0.01	11.0	12
I_y (m^4)	0.01	11.0	12
H_n (m)	3.0	4.5	10
H_b (m)	3.0	4.5	10
L_x (m)	4.0	7.0	10
L_y (m)	4.0	7.0	10
B_x (m)	15.0	50.0	100
B_y (m)	15.0	50.0	100
N	3.0	20.0	100
N_{bx}	1.0	10.0	10
N_{bx}	1.0	10.0	10
T_p	0.1	5.0	5
T (s)	0.1	3.0	5
Top Displacement (m)	0.001	2.0	2.5
Base Shear (10^4kN)	0.2	6.0	10
Base Moment (10^5kN)	0.5	10.0	10

the database generated from the nonlinear dynamic analysis results. In the neural network models, the type of back-propagation is an iterative method. The activation function is Sigmoidal Function, and the number of learning cycles is about 30000.

11. Results and Discussion

In order to test the capability of the proposed *ANN* model, the results were compared with the nonlinear dynamic analysis outcomes. The performance of the *ANN* models showed that the correlations between targets and outputs are consistent as shown in Figures (11) and (12).

The buildings with 3, 6, 10, 16 and 19 stories were used for network training. As shown in Figures (11a) and (12a), the results of training sets indicate that the *ANN* was successful in learning the correlation between the different input and outputs parameter. The results of testing sets, as shown in Figures (11b) and (12b), that the neural network was able capable of simplifying between the input and the output variables.

In validation set for ANN_1 models, all values have good relationship with nonlinear dynamic analysis results, see Figure (11b). Although, some values in the validation set showed a scatter, most of the results are in good relationship with nonlinear dynamic analysis, see Figure (12b).

12. Testing Model

For testing of data, a different plan and different number of stories were selected. The typical floor plan of the models with 5, 9, and 14 stories is shown in Figure (13). The inter-storey height is 4.00*m* for the ground and 3.50 for other stories. The width of the building along *x*-axes is $B_x = 16.0m$ and along *y*-axes $B_y = 13.0m$. The main periods of the building in two directions were calculated and compared with the ANN_1 model and the nonlinear dynamic analysis. The results are given in Tables (7) and (8)

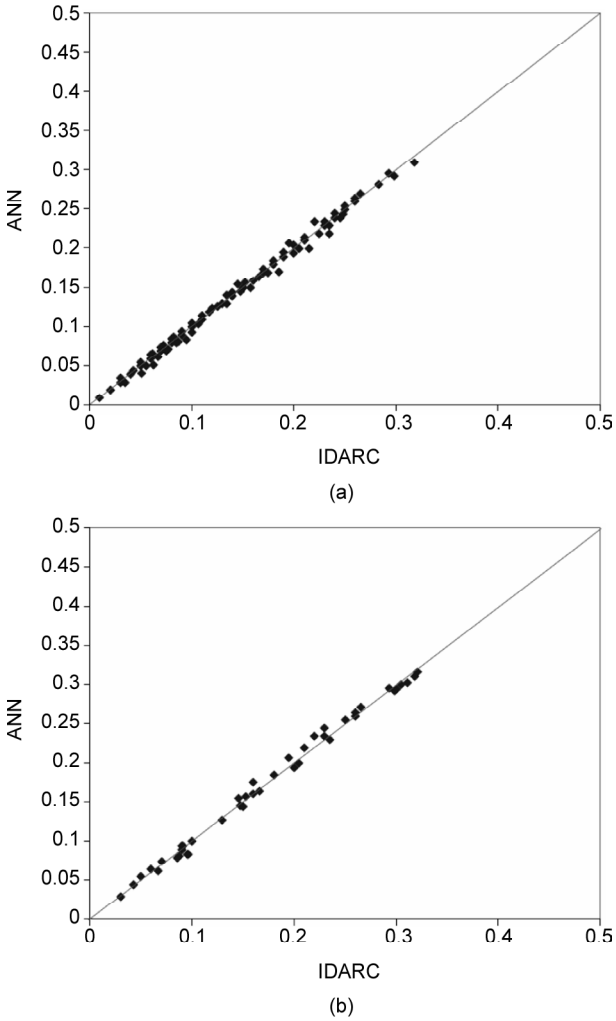

Figure 11. Performance of proposed ANN_1 model: (a) training set and (b) testing set.

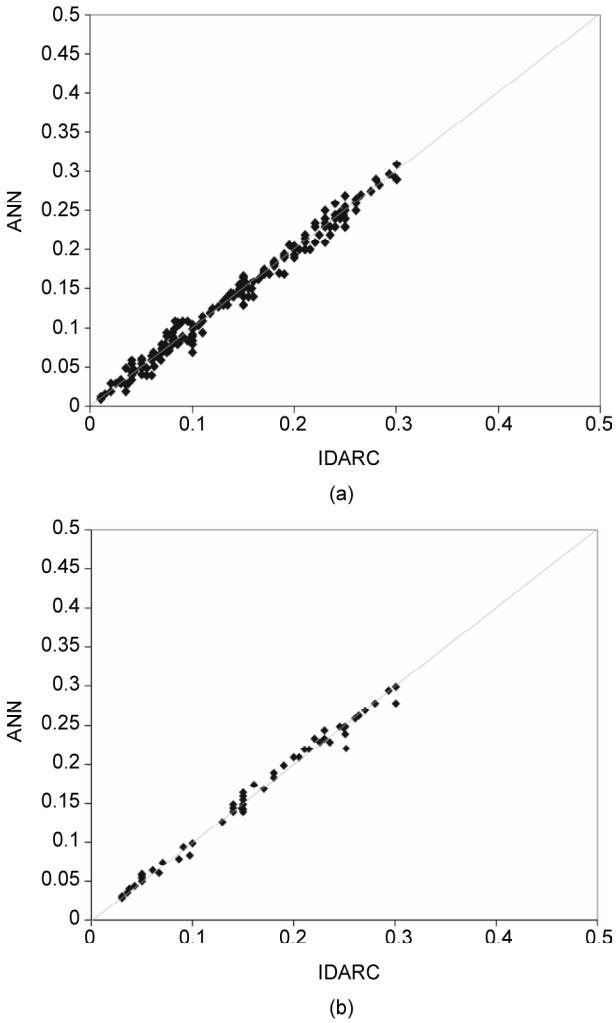

Figure 12. Performance of proposed $ANN_{2,3,4}$ model: (a) training set and (b) testing set.

and Figure (14).

The drift angles, see Figure (15), base shear forces, see Figure (16), and dissipated energy, see Figure (17), along the two directions of buildings were calculated and compared with ANN_2, ANN_3, ANN_4 models and the nonlinear dynamic analysis. Likewise, the results of analysis with *IDARC* program and *ANN* have been given in Tables (9) to (14).

The sum of the squared error (*SSE*), the root-mean-squared (*RMS*) and the absolute fraction of variance (R_2) for the testing sets of *ANN* models were tabularized in Table (15). All of the values

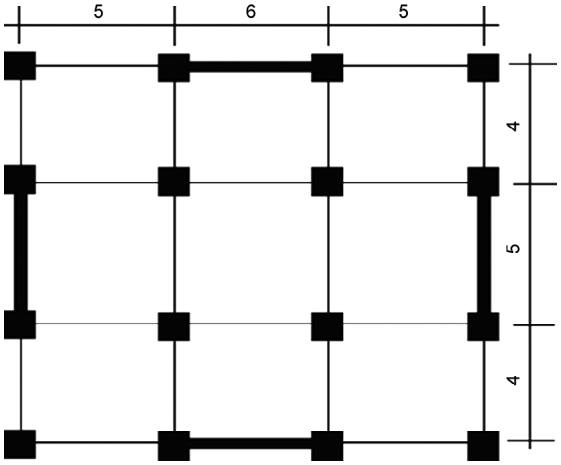

Figure 13. The typical floor plan of testing model (units: meter).

Table 7. Results of fundamental periods of ANN_1 model for the testing set in x direction (sec).

Number of Stories (x Direction)	IDARC	ANN	$\frac{ANN}{IDARC}$
3	0.2953	0.2998	1.0152
5	0.4886	0.4981	1.0194
6	0.5733	0.5563	0.9703
9	0.9856	0.9988	1.0134
10	1.0042	1.008	1.0038
14	1.4986	1.4769	0.9855
16	1.8163	1.8965	1.0441
19	1.9885	2.008	1.0098

Table 8. Results of fundamental periods of ANN_1 model for the testing set in y direction (sec).

Number of Stories (x Direction)	IDARC	ANN	$\frac{ANN}{IDARC}$
3	0.2985	0.3078	1.0311
5	0.4963	0.5091	1.0258
6	0.5893	0.5965	1.0122
9	1.056	1.088	1.030
10	1.105	1.069	0.9674
14	1.5320	1.5210	0.9928
16	1.8652	1.9028	1.0201
19	2.015	2.099	1.0417

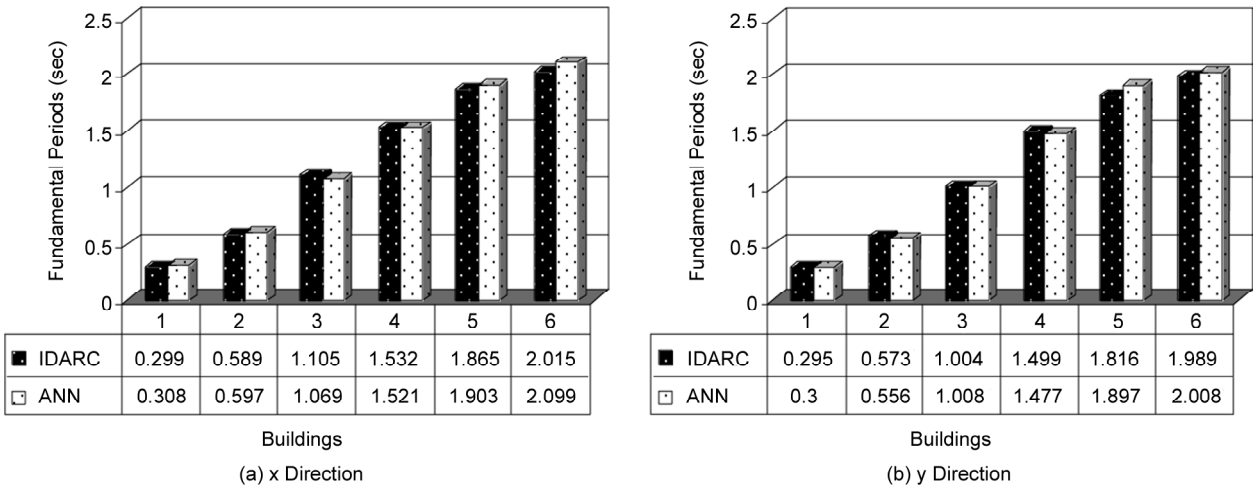

Figure 14. Fundamental periods in two directions.

established that the proposed *ANN* model is suitable for predicting the dynamic response of buildings, in terms of the fundamental periods, drift angle, base shear forces and dissipated energy, when evaluated with the results of nonlinear dynamic analysis.

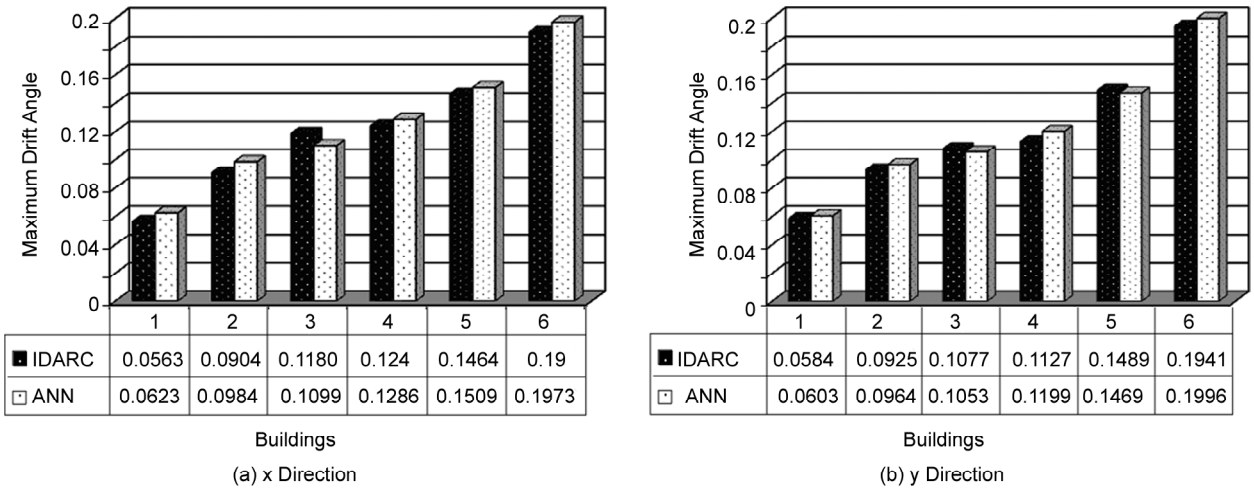

Figure 15. Drift angles in two directions.

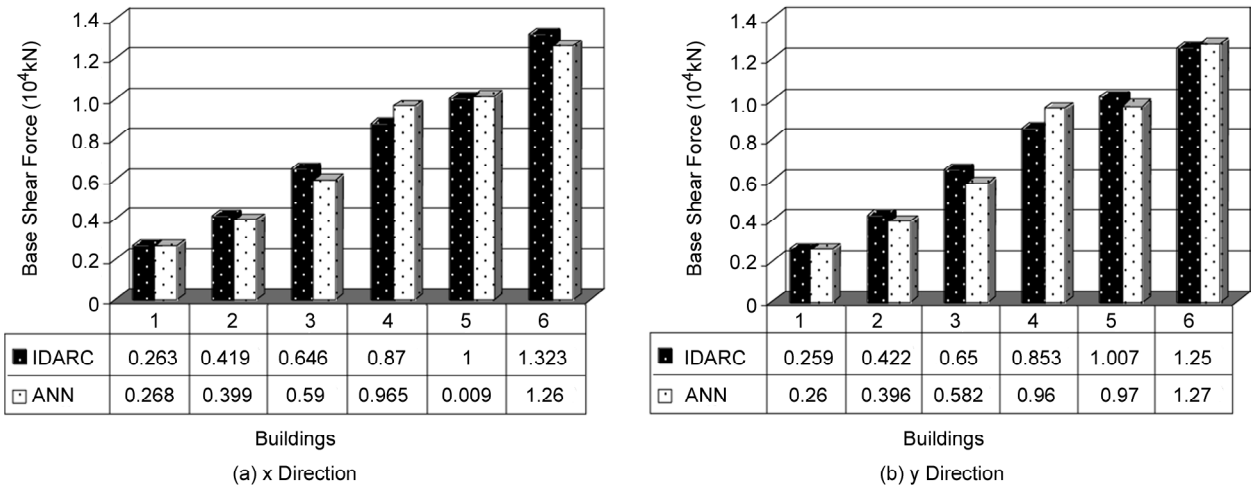

Figure 16. Base shear forces in two directions.

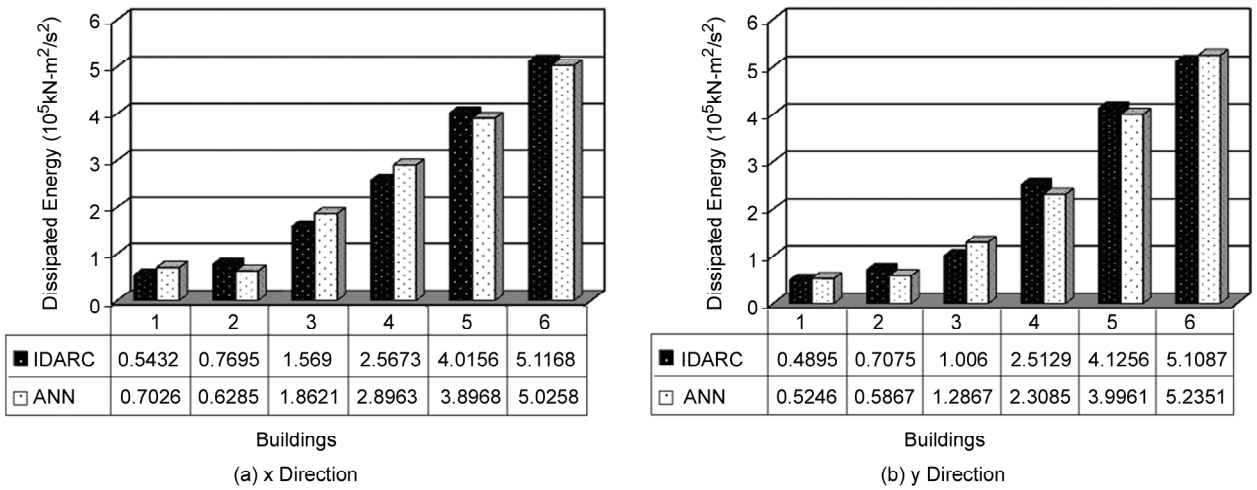

Figure 17. Dissipated energy in two directions.

The results for R_2 are 0.999689, 0.99057, 0.97895 and 0.942561 for the periods, drift angles, base shear force and dissipated energy respectively, and they show a good connection. The advantages of *ANN* over nonlinear dynamic analysis are now quite obvious as the former requires no simplifying assumptions, preliminary modeling or calibrations to name a few.

Table 9. Results of drift angles of ANN_2 model for the testing set in x direction.

Number of Stories (x Direction)	IDARC	ANN	$\frac{ANN}{IDARC}$
3	0.0563	0.0623	1.1066
5	0.0812	0.0846	1.0418
6	0.0904	0.0984	1.0884
9	0.1045	0.1088	1.0411
10	0.1186	0.1099	.9266
14	0.1240	0.1286	1.0371
16	0.1464	0.1509	1.0307
19	0.1900	0.1973	1.0384

Table 10. Results of drift angles of ANN_2 model for the testing set in y direction.

Number of Stories (x Direction)	IDARC	ANN	$\frac{ANN}{IDARC}$
3	0.0584	0.0603	1.0325
5	0.0862	0.0897	1.0406
6	0.0925	0.0964	1.0421
9	0.1036	0.1093	1.0550
10	0.1077	0.1053	0.9777
14	0.1127	0.1199	1.0638
16	0.1489	0.1469	0.9865
19	0.1941	0.1996	1.0283

Table 11. Results of base shear force of ANN_3 model for the testing set in x direction (10^4kN).

Number of Stories (x Direction)	IDARC	ANN	$\frac{ANN}{IDARC}$
3	0.2634	0.2675	1.0155
5	0.3485	0.3395	0.9741
6	0.4187	0.3989	0.9527
9	0.6052	0.6096	1.0072
10	0.6461	0.5896	0.9125
14	0.8698	0.9654	1.1099
16	1.0003	1.0086	1.0083
19	1.3229	1.2596	0.9521

Table 12. Results of base shear force of ANN_3 model for the testing set in y direction (10^4kN).

Number of Stories (x Direction)	IDARC	ANN	$\frac{ANN}{IDARC}$
3	0.2589	0.2603	1.0054
5	0.3536	0.3458	0.9779
6	0.4223	0.3957	0.9370
9	0.6132	0.6146	1.0023
10	0.6498	0.5824	0.8963
14	0.8526	0.9601	1.1261
16	1.0074	0.9701	0.9630
19	1.2504	1.2701	1.0157

Table 13. Results of dissipated energy of ANN_4 model for the testing set in x direction (10^5kN.m^2/s^2).

Number of Stories (x Direction)	IDARC	ANN	$\frac{ANN}{IDARC}$
3	0.5432	0.7026	1.2934
5	0.6856	0.6889	1.0048
6	0.7695	0.6285	0.8167
9	1.4852	1.5743	1.060
10	1.5690	1.8621	1.1868
14	2.5673	2.8963	1.1281
16	4.0156	3.8968	0.9704
19	5.1168	5.0258	0.9822

Table 14. Results of dissipated energy of ANN_4 model for the testing set in y direction (10^5kN.m^2/s^2).

Number of Stories (x Direction)	IDARC	ANN	$\frac{ANN}{IDARC}$
3	0.4895	0.5246	1.0717
5	0.6776	0.6969	1.0285
6	0.7075	0.5867	0.8292
9	1.4752	1.5836	1.0735
10	1.0060	1.2867	1.2790
14	2.5129	2.3085	0.9186
16	4.1256	3.9961	0.9686
19	5.1087	5.2351	1.0247

Table 15. The statistical values for testing building.

Statistical Values	Period	Roof Displacement	Base Shear Force	Base Bending Moment
SSE	0.002658	0.008567	0.1576	0.2943
RMS	0.012637	0.025473	0.10258	0.17586
R^2	0.999689	0.99057	0.97895	0.942561

13. Conclusions

Artificial neural networks have been widely used for simulating the behavior of complex physical phenomena applicable to many branches of science and engineering. However, there have been relatively few applications in the field of structural engineering. In this study, an *ANN* based model was applied and its predictions compared with the results obtained from nonlinear dynamic analyses. The responses of 280 different buildings were chosen and utilized as a database. 175 of these data were applied as the training set, and 105 data were used as the validation set. The *ANN* model was checked with a testing set that was not used in the training process. It was shown that the ANN-based model can successfully calculate the response of buildings in terms of the fundamental periods, maximum values of base shear forces, dissipated energy and drift angle time histories. Results of *ANN* model were actually capable and showed good generalization. This study has shown the feasibility of the potential use of *ANN* models in determining the response of buildings subjected to earthquakes. The promising results observed in the dynamic analysis of *RC* buildings indicate that the *ANN* models enable the designers to rapidly evaluate the response buildings during the preliminary design stage.

References

1. Somerville, P. (1997). "The Characteristics and Quantification of Near-Fault Ground Motion", *Proceedings of the FHWA/NCEER Workshop on the National Representation of Seismic Ground Motion for New and Existing Highway Facilities*, Burlingame, California.

2. Bertero, V.V., Mahin, S.A., and Herrera, R.A. (1978). "A Seismic Design Implication of Near-Fault San Fernando Earthquake Records", *Earthquake Engineering and Structural Dynamics*, **6**, 31-34.

3. Somerville, P. (2000). "Characterization of Near Field Ground Motions", *U.S.-Japan Workshop: Effects of Near-Field Earthquake Shaking*, San Francisco.

4. Orozco, G. and Ashford, S.A. (2002). "Effects of Large Pulses on Reinforced Concrete Bridge Columns", Pacific Earthquake Engineering Research Center, PEER Report 2002/23, College of Engineering, Univ. of California, Berkeley.

5. Iranian Code of Practice for Seismic Resistant Design of Buildings, Standard NO. 2800-05. 2005. Building and Housing Research Center.

6. Iwan, W.D., Moser, M.A., and Peng, C.Y. (1985). "Some Observations on Strong-Motion Earthquake Measurements Using a Digital Accelerograph, Bulletin of the Seismological Society of America, **75**, 1225-1246.

7. Iwan, W.D. and Chen, X.D. (1994). "Important Near-Field Ground Motion Data from the Landers Earthquake", *Proceedings of the 10th European Conference on Earthquake Engineering*, Vienna, Austria.

8. Boore, D. (2001). "Effect of Baseline Correction on Displacements and Response Spectra for Several Recordings of the 1999 Chi-Chi, Taiwan, Earthquake", Bulletin of the Seismological Society of America, **91**(5), 1199-1211.

9. Boore, D., Stephens, C.D., and Joyner, W.B. (2002). "Comments on Baseline Correction of Digital Strong Motion Data: Examples from the 1999 Hector Mine California Earthquake", Bulletin of the Seismological Society of America, **92**(4), 1543-1560.

10. Anderson, J.A. and Rosenfeld, E. (1988). "Neurocomputing: Foundations of Research", Cambridge (MA), MIT Press.

11. Caglar, N., Elmas, M., Yaman, Z.D., and Saribiyik, M. (2008). "Neural Networks in 3-Dimensional Dynamic Analysis of Reinforced Concrete Buildings", *Construction and Building Materials*, **22**, 788-800.

12. Principe, J.C., Neil, R.E., and Curt Lefebrre, W. (1999). "Neural and Adaptive System", John Wiley and Sons, Inc.

13. Park, Y.J., Reinhorn, A.M. and Kunnath, S.K. (2006). "IDARC: Inelastic Damage Analysis of Reinforced Concrete Frame-Shear-Wall Structures", National Center for Earthquake Engineering Research, Report No. NCEER-87-0008, Buffalo, NY, USA.

14. Pu, Y. and Mesbahi, E. (2006). "Application of Artificial Neural Networks to Evaluation of Ultimate Strength of Steel Panels", *Engineering Structures*, **28**(8), 1190-1196.